Physics Letters A 485 (2023) 129081

Contents lists available at ScienceDirect

Physics Letters A

journal homepage: www.elsevier.com/locate/pla

Discussion

Tuning of binding energy, polarizability and photoionization cross-section of a hydrogenic impurity in CdTe/ZnTe core-shell nanostructure by the electric field and capped matrix

S. Hértilli [a], N. Yahyaoui [a], N. Zeiri [a,*], P. Baser [b], M. Said [a], S. Saadaoui [c]

[a] Laboratory of Condensed Matter and Nanosciences (LMCN), Department of Physics, Faculty of Sciences of Monastir, 5019 Monastir, Tunisia
[b] Sivas Cumhuriyet University, Turkey
[c] Department of Physics, Faculty of Science and Arts, Mohayel Aser, King Khalid University, Abha, Saudi Arabia

ARTICLE INFO

Article history:
Received 6 June 2023
Received in revised form 20 July 2023
Accepted 15 August 2023
Available online 25 August 2023
Communicated by J.G. Lu

Keywords:
Core/shell spherical quantum dot
Photoionization cross-section
Polarizability
Impurity binding energy
Electric field

ABSTRACT

The current work describes in detail the effect of polarization charges on the electronic properties of core/shell spherical quantum dots (CSQDs) structures composed of CdTe/ZnTe semiconductors. In the calculations, energy levels and wave functions matching these levels were calculated by using the effective mass approach (EMA). Furthermore, the binding energy of a hydrogenic impurity was calculated under the variational approach. The matrix effects surrounding the CSQDs structure, the quantum dot size, the impurity, and how the applied external electric field affects the impurity binding energy (E_b), polarizability (P_a) and photoionization cross-section (PICS) are calculated and discussed in detail. The obtained results revealed that the E_b, the PICS and P_a are not only affected by the quantum parameter size but also by the capped matrix, the impurity and external electric field EF actions.

1. Introduction

Low-dimensional nanomaterials obtained by confinement particles in one dimension, two dimensions and three dimensions according to the confinement effects of the particles exhibit very different electronic and optical properties compared to bulk structures [1]. In such low-dimensional semiconductors, quantum dots (QDs) garnered great interest owing to their outstanding properties including strong quantum confinement, size-tunable photoluminescent emission, and long-term stability. Due to these properties and their high axial symmetry, other than optoelectronic applications such as QDs with different potential profiles, light-emitting diodes [2], laser technology [3], solar cells [4], live imaging, drug delivery, and cancer photodynamic therapy [5] are zero-dimensional nanomaterials used in numerous biomedical applications such as biosensors [6] for highly sensitive COVID-19 antibody detection. Hydrogenic impurities in low-dimensional structures induce bound states in the energy band, and can significantly alter the electrical, optical and transport properties, electrical conductivity, and device performance of materials. Using crystal growth techniques, impurity atoms can be added to QDs [7]. Thanks to recent advances in QD fabrication technology, core/shell quantum dots (CSQDs) have been obtained. Core-shell QDs are low-dimensional semiconductor structures obtained by covering the core with a shell of higher bandgap material. The presence of a shell coated the core ensures chemical stability to the core and passivates the non-radiative recombination sites which results in strong photoluminescence quantum yield (QY) [8]. Among all the external disturbances, we can cite the action of the EF which modifies the geometry of the structure and the localization of the charge carriers. This effect is called “Stark shift” (S. S) [9]. Optoelectronic modulators designed based on the Stark effect originating from the EF in low-dimensional structures are promising in computing technology to convert electrical signals to optical signals and optical signals to electrical signals [10].

The presence of impurities in QDs displays a considerable potential application in microelectronic and optoelectronic devices so that they can affect the electrical, optical and transport properties, including the donor hydrogenic impurity E_b under electric and dielectric environment, the PICS, and the P_a. Therefore, the influence of the impurity atom on the optoelectronic properties, binding energy states and other physical qualifications of QDs of various shapes has been extensively studied in the literature [11–15]. Research on the impurity position and the applied EF intensity on the E_b of the impurity atom are remarkable.

* Corresponding author.
E-mail address: zeirinabil@gmail.com (N. Zeiri).

https://doi.org/10.1016/j.physleta.2023.129081
0375-9601/

In this context, the authors in ref. [16] investigated how a shallow donor's energy in a spherical quantum crystallite at any location changes its quantum size, impurity location, and EF. It was observed that the energy increased as the impurity moved away from the center at a given QD size. In addition, it was proved that as the uniform EF increases, the energy of the impurity in the center of the crystal decreases, and the energy change for the impurity placed in the z direction outside the center changes with the angle between the EF and the z direction. The authors in ref. [17] investigated the effects of impurity location, strength and direction of the EF, and size on the E_b of a hydrogenic impurity in a quantum disk. It was calculated that the E_b increased considerably when the impurity was at the disk edge and the EF was in the opposite direction of the impurity. In addition, A. L. Morales et al. have investigated theoretically the simultaneous effect of pressure and EF on the BE as a function of impurity position in a GaAs-(Ga, Al)As quantum well in reference [18], they concluded that it a BE trend, similar to the one obtained by the application of an EF alone. Whereas, the pressure effect then produces an additional displacement ent of the BE in the opposite direction to the applied EF. Meanwhile, the authors in reference [19], have studied the EF effect on the states of a donor impurity in rectangular cross-section vacuum/GaAs/vacuum quantum-well wires using the EFM within a variational scheme, they showed that the presence of the electric field breaks down the degeneracy of states for impurities symmetrically positioned within the structure, and that the geometric confinement and the electric field are determinants for the existence of bound excited states in these structures. Moreover, the authors in reference [20] have carried out a comparative study of the effect of hydrostatic pressure and temperature on the shallow-impurity-related optical absorption spectra in GaAs-$Ga_{1-x}Al_xAs$ single and double quantum wells, based on a variational technique within the effective mass approximation. They showed a pressure-dependent red shift and a temperature-dependent blue shift in the optical absorption spectra. As well as in the previous studies, Sotirios et al. [21] have found that the optoelectronic properties of QD are greatly influenced by the impurity and EF effects. Authors ref. [22] calculated the electronic features of hydrogenic impurities in CSQDs consisting of CdSe/ZnS and ZnS/CdSe semiconductors surrounded by wide band gap dielectric materials. As a result of the calculations, it was shown that the hydrogenic impurity E_b can be adjusted according to the size of the QDs, the location of the impurity, and the properties of the matrix surrounding the QD. On the other hand, Chafai et al. [23]. When the authors investigated the simultaneous effects of the impurity, EF and host medium using the variational approach, they proved that the density of probability and the Stark shift are highly dependent on the matrices surrounding the CSQD structure, the impurities in the structure, and the EF applied. PICS is a property that describes the optical properties of the impurity atom in the QD structure. That's why the impact of applied EF on the PICS in semiconductor nanostructures with various shapes is actively studied theoretically [24–27]. Şahin et al. [28] investigated the dependence of the PICS, electronic energies and E_b of a multilayer spherical QD with a hydrogenic impurity in its center. It was shown that PICS and E_b are highly affected by layer thickness and photon energies. Recently, Shi et al. [29] have evaluated, under the EMA and by using a variational method, the S. S of a donor impurity E_b and PICS in core/shell ellipsoidal QDs under a uniform EF. Their theoretical model reveals that the S. S is affected by the shape and the QD size and increases nearly linearly with the raising F. It is also found that for a spherical shape under the condition F = 0 kV/cm, the PICS will disappear when the impurity is in the center. Recently, Fakkahi et al. [30] investigated size effects and external EF attribution on E_b, P_a and PICS of hydrogenic impurity in multilayer spherical quantum dots (MSQDs).

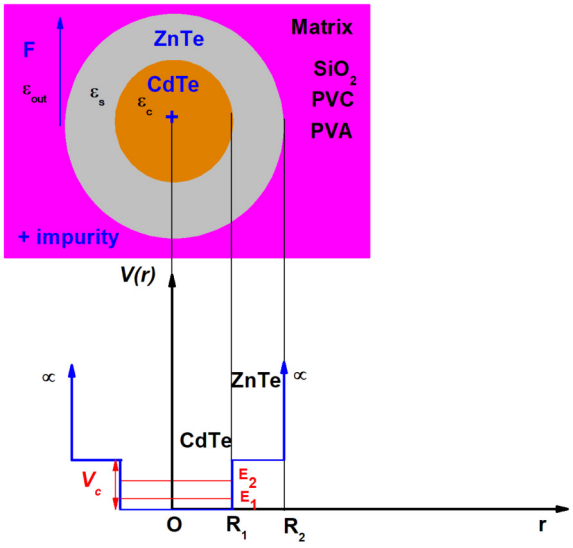

Fig. 1. Schematic diagram of CdTe/ZnTe CSQDs heterostructure embedded in three D. M.

Their findings showed that QD size and applied EF strength significantly affect E_b, P_a, and PICS.

The article examines the theoretical investigation of the hydrogenic donor confined with spherical CSQDs embedded in a dielectric Matrix (D.M) under the variational approach and using EMA. We focus on the behavior of impurity BE, S. S and P_a under the influence of both EF power and QD size, as well as photon energy-dependent changes of PICS for different EF strength values.

The research is organized as follows. Chapter 2 describes the theoretical model and computation. In Chapter 3, the calculation results and the graphs obtained are interpreted in detail. Finally, the results are briefly summarized in section 4.

2. Model and theory

In this research, the electronic and optical properties of a hydrogenic impurity located at the center of the confined structure in CdTe/ZnTe CSQDs with core radius R_1 and shell radius R_2 were investigated. The CSQDs structure is submerged in different D. M (PVA, PVC, SiO_2), and subjected to an external EF $\vec{F} = F\vec{u}_z$. The understudied core/shell structure is schematically presented in Fig. 1. The Hamiltonian of the system, which consists of an electron in the CSQDs structure under the EF and a hydrogenic donor in the center, is written with EMA as:

$$\left(\widehat{H}_0 + \widehat{H'}\right)\Psi_{n,l}\left(\vec{r}\right) = E_{n,l}\left(\vec{r}\right)\Psi_{n,l}\left(\vec{r}\right) \tag{1}$$

Here, the Hamiltonian EF is defined by $\widehat{H}_0$ is for an electron confined in the CdTe/ZnTe CSQDs-Matrix system in the absence of an impurity atom.

$$\widehat{H}_0 = -\frac{\hbar^2}{2m_j^*}\Delta + V_{conf}\left(\vec{r}\right) + \sum(R_s) \tag{2}$$

Here, $\hbar$ is the Planck constant, m_j^* defines the effective mass of the electron for the nucleus and the shell, and $V_{conf}\left(\vec{r}\right)$ defines the confinement potential. The confinement potential is given as:

$$V_{conf}\left(\vec{r}\right) = \begin{cases} 0 & 0 < r \le R_1 \\ V_c & R_1 < r \le R_2 \\ \infty & r > R_2 \end{cases} \tag{3}$$

and m_j^* in different regions is defined as:

$$m_j^* = \begin{cases} m_{CdTe}^* & r < R_1 \\ m_{ZnTe}^* & R_1 < r \leq R_2 \end{cases} \quad (4)$$

And $\sum(R_s)$ designates the electron self-polarization potential induced by charging the QD with a host medium given in Refs. [31,32]:

$$\sum(R_s) = \frac{e^2}{4\pi\varepsilon_0 R_s}\left[\frac{1}{2}\left(\frac{1}{\varepsilon_{out}} - \frac{1}{\varepsilon_{in}}\right) + \frac{0.466}{\varepsilon_{in}}\left(\frac{\varepsilon_{in} - \varepsilon_{out}}{\varepsilon_{in} + \varepsilon_{out}}\right)\right] \quad (5)$$

Where $\varepsilon_{in} = \sqrt{\varepsilon_{CdTe}.\varepsilon_{ZnTe}}$ and ε_{out} are the dielectric constants of CdTe/ZnTe CSQD and the D. M., respectively.

The Hamiltonian which describes the simultaneous action of the external EF and the coulombic interaction in Eq. (1), is written:

$$\widehat{H'} = U\left(\vec{r}\right) + eF.r.\cos(\theta) \quad (6)$$

e is the elementary charge of the electron and $U\left(\vec{r}\right)$ is the Coulomb potential due to the impurity-related coulombic interaction. For an on-center impurity, it can be written as [31,32]:

$$U\left(\vec{r}\right) = -\frac{e^2}{4\pi\varepsilon_{in} r} - \frac{e^2(\varepsilon_{in} - \varepsilon_{out})}{4\pi\varepsilon_{in}\varepsilon_{out} R_2} \quad (7)$$

Where the first term represents the Coulomb interaction between the ion impurity and electron and the second arises from the interaction between the CSQD and D. M. The wave functions of $\widehat{H}_0$ can be written in spherical coordinates as $\Psi_{n,l}^0(r,\theta,\varphi) = R_{n,l}^0(r).Y_{l,m}(\theta,\varphi)$ without taking into account the EF and impurity effect. The solution of the radial part $R_{n,l}^0(r)$ are the spherical Bessel function and Hankel functions of the first and the second kinds taken from [33]:

$$R_{n,l}^0(r) = \begin{cases} A_1 j_l\left(k_{nl,1} r\right) & 0 < r \leq R_1 \\ B_1 h_l^{(+)}\left(ik_{nl,1} r\right) + B_2 h_l^{(-)}\left(ik_{nl,2} r\right) & R_1 < r \leq R_2 \\ 0 & r > R_2 \end{cases} \quad (8)$$

Here $k_{nl,1}$ and $k_{nl,2}$ are eigenvalue constants while A_1, B_1 and B_2 are normalized constants. The boundary continuity conditions for these functions are detailed in Refs. [33,34].

$$k_{nl,1} = \frac{\sqrt{2m_{CdTe}^*(E_{n,l} - \sum(R_s))}}{\hbar^2};$$
$$k_{nl,2} = \frac{\sqrt{2m_{ZnTe}^*\left(V_c + \sum(R_s) - E_{n,l}\right)}}{\hbar^2} \quad (9)$$

Combining the influence of the EF and the trial wave function for the impurity state can be written as [29]:

$$R_{\lambda,\eta}(r) = R_{n,l}^0(r)\, e^{-\lambda r} e^{-\eta r cos\theta} \quad (10)$$

In Eq. (10), we recall that λ and η are variational parameters introduced to indicate the degree of spatial correlation between electron and impurity and the influence of the EF, respectively. Considering the perturbation theory, the ground state energy of the impurity can be minimizing the expectation energies [29,35,36,38] concerning λ and η:

$$E = \min_{\lambda,\eta} \frac{\left\langle \Psi_{n,l}(r,\theta,\varphi) \mid \widehat{H} \mid \Psi_{n,l}(r,\theta,\varphi) \right\rangle}{\left\langle \Psi_{n,l}(r,\theta,\varphi) \mid \Psi_{n,l}(r,\theta,\varphi) \right\rangle} \quad (11)$$

Where $\widehat{H}$ is the total Hamiltonian. The E_b of the hydrogenic impurity is defined as the difference between the ground state energy of the system without and with the impurity, and can be written as [37]:

$$E_b = E_0 - E \quad (12)$$

We define P_a as follows:

$$P_a = -\frac{e}{F}\Big(\left\langle \Psi_{n,l}(r,\theta,\varphi) \mid r \mid \Psi_{n,l}(r,\theta,\varphi)\right\rangle_{F\neq 0} - \left\langle \Psi_{n,l}(r,\theta,\varphi) \mid r \mid \Psi_{n,l}(r,\theta,\varphi)\right\rangle_{F=0}\Big) \quad (13)$$

The CSQDs system is encapsulated in a D. M. and subjected to a uniform EF. We assume that our nano-heterostructure is a uniform host medium with permittivity ε_{in} and immersed in the D. M with the permittivity ε_{out}. The authors in ref. [38] have shown that in a spherical structure, the EF inside the dot F_d is related to the outer by the expression:

$$F_d = \frac{3\varepsilon_{out}}{2\varepsilon_{out} + \varepsilon_{in}} F_a \quad (14)$$

Where F_a is the uniform electric field submitted when the quantum dot is embedded in a D.M.

The PICS is defined as the probability of ionization of the electron bound to a hydrogenic impurity under external optical excitation. In this survey, we consider the PICS related to the difference between ground states with and without impurity. In the dipole approximation, the PICS is expressed as [25,39–41]:

$$\sigma(\hbar\omega) = \left[\left(\frac{F_{eff}}{F_0}\right)^2 \frac{n_r}{\varepsilon_{in}}\right] \frac{4\pi^2}{3} \beta_{FS} \hbar\omega \sum_f \left|M_{if}\right|^2 \delta\left(\Delta E_{if} - \hbar\omega\right) \quad (15)$$

In the above equation, $n_r = \sqrt{\varepsilon_{in}}$ is the refractive index change, ε_{in} is the permittivity of the medium, $\beta_{FS} = \frac{e^2}{4\pi\varepsilon_0\hbar c}$ is the fine structure constant and $\hbar\omega$ is the incident photon energy. $\frac{F_{eff}}{F_0}$ is the ratio of the effective EF on the impurity F_{eff} to the average EF of the medium F_0, we assume that $\frac{F_{eff}}{F_0} = 1$ [42,44,45] because it does not affect the PICS shape. ΔE_{ij} is the difference in energy. The term $M_{ij} = F_d\left\langle \Psi_i \mid r \mid \Psi_f \right\rangle$ designates the dipole matrix element between the initial and final states with and without impurity. As is usually done, the δ-function is substituted by a narrow Lorentzian function that is:

$$\delta\left(\Delta E_{if} - \hbar\omega\right) = \frac{\hbar\Gamma}{\pi\left[\left(\hbar\omega - \left(\Delta E_{if}\right)\right)^2 + (\hbar\Gamma)^2\right]} \quad (16)$$

Where $\Gamma = \frac{1}{\tau}$ is the hydrogenic impurity line width.

3. Results and discussion

In this part, the results of the electronic and optical properties evaluated in this paper have been computed numerically using the variational method. The calculations were performed for a CdTe/ZnTe CSQDs system. The impact of the dielectric environment on the energy is considered via the self-energy term introduced previously in Eq. (5). By the way, Table 1 and Table 2 provide the precise physical parameters used in the computation.

3.1. BE and S. S of hydrogenic donor impurity confined in CSQDs structure under applied EF and dielectric environment

First, we start by looking at the behavior of the E_b versus the nanodot size. Fig. 2 presents the variation of the donor ground state E_b versus core/shell radii R_1/R_2 for three D. M (PVA, PVC,

Table 1
Recommended parameter values for CdTe and ZnTe used in our computations.

Materials	Effective mass (m^*/m_0)	Dielectric constant (ε_r)	Energy gap E_g (eV)	Conduction band offset (V_{0e}) (eV) CdTe/ZnTe
CdTe	0.095 [41]	10.2 [41]	1.50 [55]	-
ZnTe	0.12 [41]	9.7 [41]	2.26 [55]	0.67 [41]

Table 2
Various D. M. utilized in this work and their dielectric constants.

D.M	Dielectric constant ε_{out}
SiO_2	3.9 [42,43]
PVC	4 [42,43]
PVA	14 [42,43]

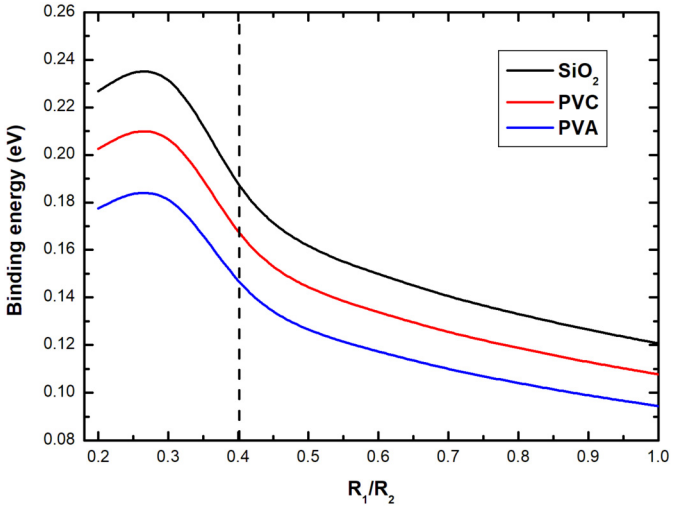

Fig. 2. The BE versus the core/shell radii R_1/R_2 for three coated D. M.

SiO_2). It is clear that the BE is highly influenced by the core size modification. BE starts to increase as electron and impurity get closer to each other as we go to the small size regime in QD. At a certain value of R_1/R_2 ($R_1/R_2 \cong 0.26$) BE reaches a maximum value and at values less than $R_1/R_2 \cong 0.26$, a decrease in BE is observed. Because the quantum confinement effects are very strong as the size decreases, the high-energy electron infiltrates the ZnTe shell region. BE starts to diminish as the distance between the electron and the impurity increases. As the quantum confinement effects decrease as the R_1/R_2 increase to large values, the impurity and electron move away from each other and the E_b decreases. As the core size increases, the BE value approaches the bulk value of the CdTe semiconductor. Our numerical results correspond well to those of the Refs. [22,46]. It is seen that the dielectric mismatch effect changes the BE value in each region. However, the change of BE with respect to R_1/R_2 is similar in general interpretations in all three Matrices. But different matrix elements change the value of E_b considerably. Indeed, for instance with $R_1/R_2 = 0.4$, $E_b = 0.1975$ eV for SiO_2 (silicon dioxide) with permittivity $\varepsilon_{out} = 3.9$, $E_b = 0.1775$ eV in the case of PVC (polyvinyl chloride) with permittivity $\varepsilon_{out} = 4$ while $E_b = 0.1575$ eV for PVA (poly-vinyl alcohol) with permittivity $\varepsilon_{out} = 14$. It is seen that E_b decreases as the permittivity of the capped matrix increases. This is in line with our expectations. Because as the permittivity increases, the Coulomb interaction decreases significantly and lower binding energies are obtained. The obtained results are compared with those available in the literature [47–49]. Adjusting the dot

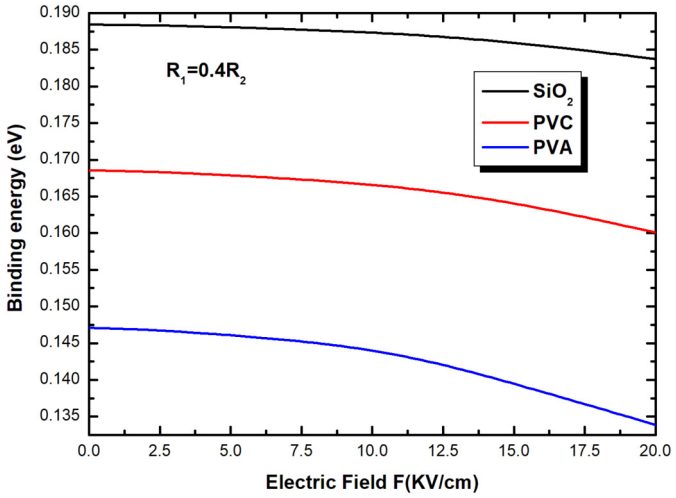

Fig. 3. The BE versus the applied EF strength for three coated D. M. with a fixed ratio $R_1/R_2 = 0.4$.

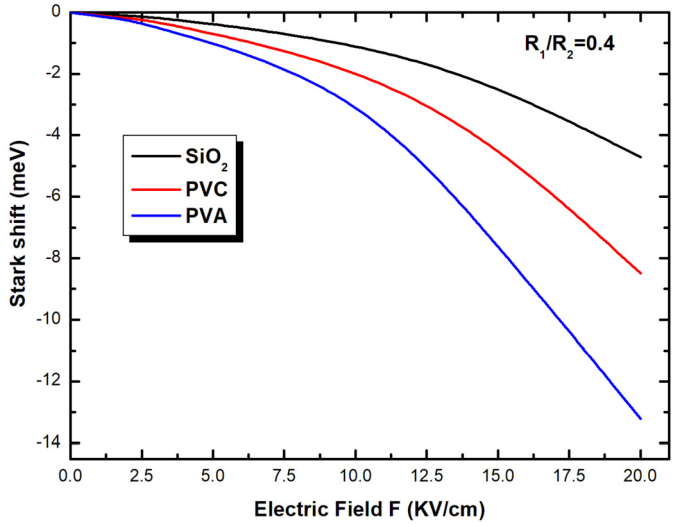

Fig. 4. The S. S versus the EF strength for three surrounding D. M. with a fixed ratio $R_1/R_2 = 0.4$.

size and the suitable choice of the D. M. can offer the possibility of modulating the energy transition in a QD-matrix system.

In Fig. 3, we have plotted the variation of the ground state E_b of an on-center impurity versus external EF intensity for a fixed value of $R_1/R_2 = 0.4$ for different D. M. From the plot, as can be seen, in all the curves, the BE maximum is situated at F = 0 kV/cm. As the F increases, the BE significantly decreases from a maximum to a minimum value corresponding to F = 20 kV/cm. This behavior is due to the impact of the external EF intensity which breaks the symmetry and can only reinforce the asymmetric. Indeed the action of the EF in this case lifts the degeneracy, decreases the energy levels and therefore the BE. A similar behavior is found in the study associated with spherical CSQDs nanostructure by E.C. Niculescu et al. [50] when the authors investigated, taking into consideration the dielectric confinement, the impact of an applied EF on the impurity levels and PICS in a CdSe/ZnS core/shell nanodot. They deduced that for donors placed at the QD center, the distance electron impurity increase by the EF effect which decreases the coulomb interaction. In order to understand the EF strength influence on the displacement of the BE, we have plotted in Fig. 4 the S. S versus EF strength for three immersed matrices for a fixed value of $R_1/R_2 = 0.4$. However, the S. S is defined by:

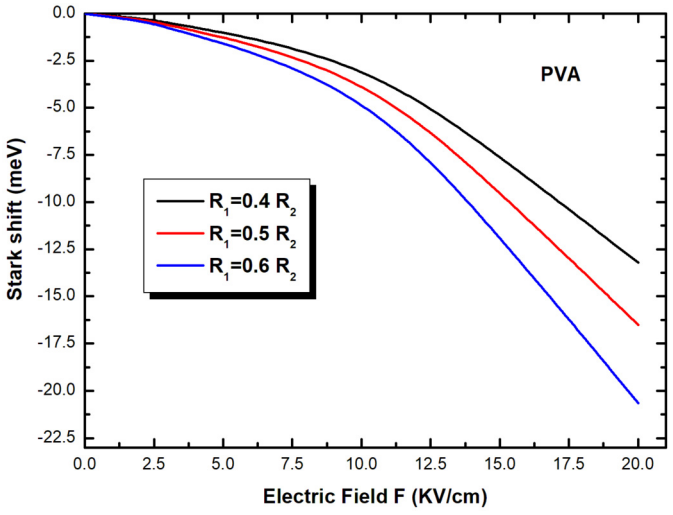

Fig. 5. The S. S versus the EF strength for different sizes of core radius in the case of the PVA matrix.

the BE difference with and without applied EF intensity ($\Delta E_b = E_b$ (F $\neq$ 0) $- E_b$ (F = 0). The S. S decreases quadratically with applied EF strength for various D. M as expected.

It is observed that the S. S effect in SiO_2 matrix element with a lower dielectric constant $\varepsilon_{out} = 3.9$ is less than in PVC and PVA matrix environments with large dielectric constants. When the dielectric effect is weak, the charge distribution is less susceptible to the EF, since the Coulomb potential effect is stronger. In all three SiO_2, PVC, and PVA matrices, the S. S becomes larger as the EF increases because as the EF increases, the Coulomb interaction decreases. Therefore, as the EF increases, the E_b decreases. From our results, one may see that the higher permittivity of the matrix coated the Core-Shell QD, the stronger the S. S due to the strong confinement effect. The obtained results are similar to previous works [51,52].

Fig. 5 shows the S. S changes versus EF intensity for three sizes of the core radius when the CSQDs structure is coated in a PVA matrix with a dielectric constant $\varepsilon_{out} = 14$. We remark that the S. S is not only influenced by EF but also by the dot size. On the other hand, as the R_1/R_2 ratio decreases, we would expect the S. S to present an almost linear behavior with EF. In fact, at smaller QD dimensions, the S. S is less sensitive to EF density due to the quantum confinement effect. Our analyses are in good accordance with Ref. [53].

3.2. Polarizability of on-center impurity confined in the CSQDs structure

In the following discussions, our investigation will focus on the P_a. Fig. 6, we have depicted the dependence of the P_a on the R_1/R_2 for the studied structure for various encapsulating D. M (PVA, PVC, SiO_2) and for a given value of EF F = 5 kV/cm. From this curve, it is obvious that the P_a is strongly influenced by the QDs size. All the curves in this figure follow the same trend, the P_a increases as the core size increases. All curves in this figure follow the same trend, as the core size increases, the polarizability increases as the quantum confinement effect weakens. Conversely, as the size diminishes, the polarization of the impurity diminishes due to the strong confinement effect. This behavior is consistent with the results in ref. [22]. Moreover, we can also see from the figure that the capped matrix with a higher dielectric constant exhibits a strong P_a, whereas the encapsulated matrix with a lower dielectric constant exhibits a weaker P_a. This conclusion has been established by Zeiri et al. [54] when the authors studied theoretically the impact of the quantum parameter size and the capped matrix on the P_a

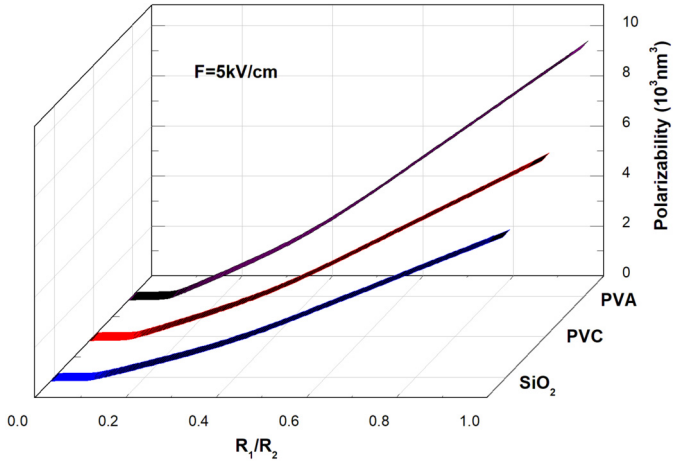

Fig. 6. The Polarizability on the core/shell radii R_1/R_2 for three capped D. M. at a given EF F = 5 KV/cm.

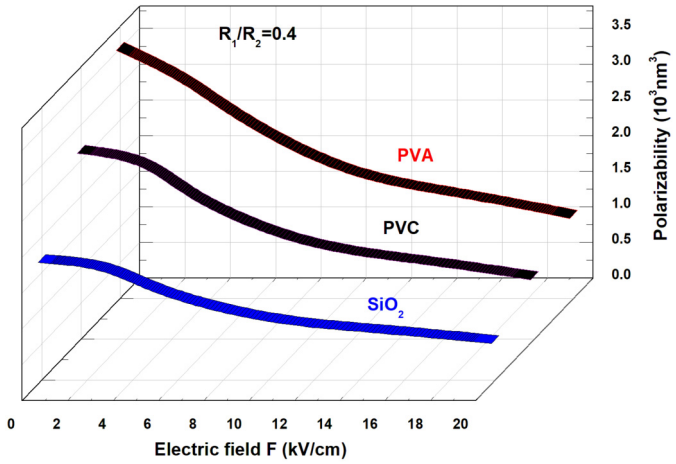

Fig. 7. The Polarizability on the EF strength for three capped D.M with a fixed ratio $R_1/R_2 = 0.5$.

and PICS of spherical CdS/ZnS CSQDs. They indicated that the QDs immersed in a matrix having a higher D. M (case of PVA) exhibit a significant P_a.

Fig. 7 is devoted to the investigation of the P_a. This figure shows the dependence of P_a versus EF strength for several matrices (PVA, PVC, SiO_2) with $R_1/R_2 = 0.5$. It is evident to notice that the P_a sensitively depends on the applied EF and dielectric environment. From the observation of these curves, one can notice that the P_a has a maximum value when F = 0 kV/cm. Additionally, it is also clear that by increasing the EF strength the P_a diminishes, and it is stronger in the case of the PVA matrix. As can be seen from the plot, the EF shifts the maximum values to a smaller core radius and reduces the intensity of the maximum P_a. This result is consistent with other published work [55].

3.3. PICS of on-center impurity confined in the CSQDs structure

Finally, we present the PICS. Fig. 8 shows the PICS versus incident $\hbar\omega$ (eV) and this is for the three different possible encapsulating matrices with $R_1/R_2 = 0.4$ under the condition F = 0 kV/cm. As can be seen from the graph, as the permittivity of the matrix-coated QD increases, the PICSs increase and their resonant amplitudes move towards lower energies. That is, the resonant frequencies are redshifted with increasing permittivity. While the increase in amplitudes is explained by the change of the dipole matrix elements, the redshift is related to the transition energies.

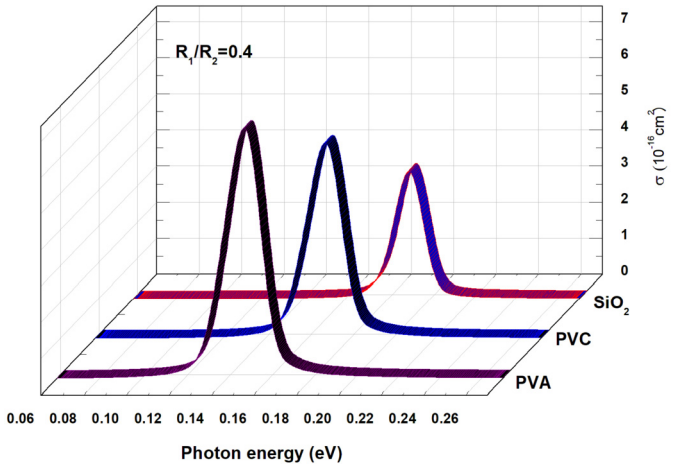

Fig. 8. The PICS variation versus the incident photon energy for three encapsulating D. M. with an affixed ratio $R_1/R_2 = 0.4$ under the condition F = 0 KV/cm.

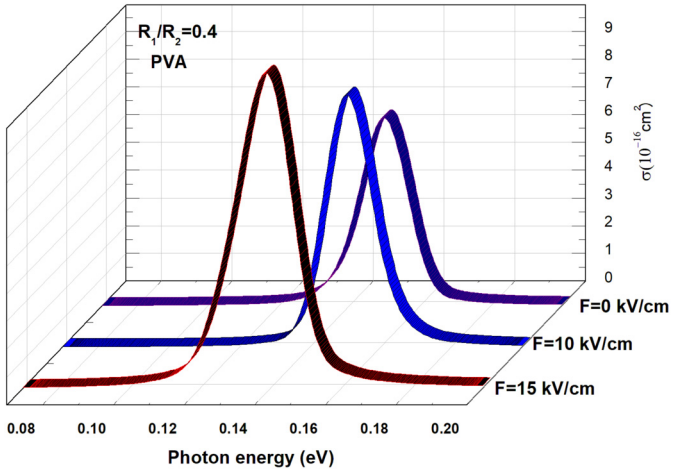

Fig. 9. The PICS variation versus the incident photon energy for different values of the EF strength with a fixed ratio $R_1/R_2 = 0.4$ in the case of the PVA matrix.

This shift can be explained as follows: Two cases can be treated here: When we deal with the SiO_2 matrix, in this case $\varepsilon_{in} > \varepsilon_{out}$ and the local field factor F < 1 which results in weaker PICS. The situation is just reversed when we deal with the PVA matrix, in this case, $\varepsilon_{in} < \varepsilon_{out}$ and the local field factor F > 1 induces an increase in $M_{i,j}$ and a stronger PICS magnitude results in a better overlap between wave functions observed. The same outcome has been established by the authors in Refs. [51,56,57].

We have extended our study to understand the impact of EF on optical properties. Fig. 9 depicts the PICS versus $\hbar\omega$ (eV) for different values of the EF strength for $R_1/R_2 = 0.4$ and the coated matrix is PVA.

The first point that draws attention in Fig. 9 is that as the applied EF intensity increases, the PICS resonant amplitudes increase and the resonant energies shift towards lower energies. In other words, as EF increases, the resonant frequencies are redshifted. The reason for these changes that occur with the increasing EF is that the applied EF disrupts the symmetry of the structure and thus strengthens the asymmetry of the structure.

The reason for the redshift of resonant frequencies with increasing EF density is that the difference between electron energy levels decreases as EF increases. As the applied EF increases, the increase in PICS amplitudes is related to the $M_{i,j}$, and in this case, we can say that $M_{i,}$ increases as EF increases.

As shown from this figure, the PICS reaches its maximum values for F = 15 kV/cm. Note that the PICS can be controlled by adjusting the applied EF strength, the D. M and the quantum parameter size. These characteristics can be exploited to design some device applications like QD infrared photodetectors.

4. Conclusion

In summary, we have studied the BE, P_a and PICS of a hydrogenic impurity confined in a CdTe/ZnTe CSQDs using the vibrational method under the framework of the EMA. The E_b, the S. S, the P_a and the PICS are discussed within the impact of EF strength and taking into account the dielectric mismatch. Hydrogenic impurity E_b, S. S, P_a and PICS are discussed under the influence of EF force and considering dielectric mismatch and QD dimension.

To summarize the important results obtained briefly:

i) The binding energy of the hydrogenic donor impurity appeared to vary considerably depending on the size of the CSQDs. As the size decreases, E_b is maximum at a certain value, and if the size decreases further from this value, the E_b decreases as the electron leaks into the shell region. In addition, it was observed that E_b of CdTe approached the bulk value as the core radius increased. **ii)** It was determined that as the dielectric constant of the matrix coated the CSQDs and the EF applied to the structure increased, the E_b decreased. **iii)** It was observed that the S. S was less sensitive to EF as the permittivity of the matrix coated the CSQDs decreased, and it was observed that as the EF increased for all the matrix elements, the S. S was stronger. **iv)** The impurity polarization weakens as the core size and EF intensity increase, while it becomes stronger as the permittivity of the matrix element coated in the CSQDs increases. **v)** As for PICS, as the EF and the dielectric constant of the matrix coated the CSQDs increase, the PICS resonant amplitudes increase, while the PICS resonant frequencies are redshifted.

In terms of PICSs, the EF and the permittivity of the matrix-coated structure can be alternatives to each other. These variable parameters are important for the optimum of the structure. In this study, we hope that the examination of the optical and electronic properties of the hydrogenic impurity with the dielectric constant, applied EF and QD dimension will lead to experimental studies and new device designs.

CRediT authorship contribution statement

S. Hértilli: Formal analysis. **N. Yahyaoui:** Methodology. **N. Zeiri:** Writing – original draft. **P. Baser:** Writing – review & editing. **M. Said:** Supervision. **S. Saadaoui:** Visualization.

Declaration of competing interest

The authors declare that they have no known competing financial interests or personal relationships that could have appeared to influence the work reported in this paper.

Data availability

No data was used for the research described in the article.

Acknowledgements

The authors extend their appreciation to the Deanship of Scientific Research at King Khalid University for funding this work through large group Research Project under grant number RGP2/19/44.

References

[1] R.G. Chaudhuri, S. Paria, Core/shell nanoparticles: classes, properties, synthesis mechanisms, characterization, and applications, Chem. Rev. 112 (2012) 2373–2433, https://doi.org/10.1021/cr100449n.

[2] Z. Yang, M. Gao, W. Wu, X. Yang, X.W. Sun, J. Zhang, H.C. Wang, R.S. Liu, C.Y. Han, H. Yang, W. Li, Recent advances in quantum dot-based light-emitting devices: challenges and possible solutions, Mater. Today 24 (2019) 69–93, https://doi.org/10.1016/j.mattod.2018.09.002.

[3] Y.S. Park, J. Roh, B.T. Diroll, R.D. Schaller, V.I. Klimov, Colloidal quantum dot lasers, Nat. Rev. Mater. 6 (2021) 382–401, https://doi.org/10.1038/s41578-020-00274-9.

[4] A.S. Sadhu, Y.M. Huang, L.Y. Chen, H.C. Kuo, C.C. Lin, Recent advances in colloidal quantum dots or perovskite quantum dots as a luminescent downshifting layer embedded on solar cells, Nanomaterials 12 (2022) 985, https://doi.org/10.3390/nano12060985.

[5] A.A.H. Abdellatif, M.A. Younis, M. Alsharidah, O. Al Rugaie, H.M. Tawfeek, Biomedical applications of quantum dots: overview, challenges, and clinical potential, Int. J. Nanomed. 17 (2022) 1951–1970, https://doi.org/10.2147/IJN.S357980.

[6] Y. Zheng, K. Song, K. Cai, L. Liu, D. Tang, W. Long, B. Zhai, J. Chen, Y. Tao, Y. Zhao, S. Liang, Q. Huang, Q. Liu, Q. Zhang, Y. Chen, Y. Liu, H. Li, P. Wang, K. Lan, H. Liu, K. Xu, B-cell-epitope-based fluorescent quantum dot biosensors for SARS-CoV-2 enable highly sensitive COVID-19 antibody detection, Viruses 14 (2022) 1031, https://doi.org/10.3390/v14051031.

[7] E. Feddi, A. Zouitine, A. Oukerroum, F. Dujardin, E. Assaid, M. Zazoui, Size dependence of the polarizability and Haynes rule for an exciton bound to an ionized donor in a single spherical quantum dot, J. Appl. Phys. 117 (2015) 064309, https://doi.org/10.1063/1.4907760.

[8] I. Hemdana, M. Mahdouani, R. Bourguiga, Investigation of the radiative lifetime in core-shell CdSe/ZnS and CdSe/ZnSe quantum dots, Physica B, Condens. Matter 407 (2012) 3313–3319, https://doi.org/10.1016/j.physb.2012.04.002.

[9] O. Mommadi, A. El Moussaouy, M. El Hadi, M. Chnafi, Y.M. Meziani, C.A. Duque, Stark shift and exciton binding energy in parabolic quantum dots: hydrostatic pressure, temperature, and electric field effects, Philos. Mag. 101 (2021) 753–775, https://doi.org/10.1080/14786435.2020.1862430.

[10] N.C. Helman, J.E. Roth, D.P. Bour, H. Altug, D.A.B. Miller, Misalignment-tolerant surface-normal low-voltage modulator for optical interconnects, IEEE J. Sel. Top. Quantum Electron. 11 (2005) 338–342, https://doi.org/10.1109/JSTQE.2005.845613.

[11] D.S. Chuu, C.M. Hsiao, W.N. Mei, Hydrogenic impurity states in quantum dots and quantum wires, Phys. Rev. B, Condens. Matter 46 (1992) 3898–3905, https://doi.org/10.1103/physrevb.46.3898.

[12] V.A. Holovatsky, O.M. Makhanets, O.M. Voitsekhivska, Oscillator strengths of electron quantum transitions in spherical nano-systems with donor impurity in the center, Physica E, Low-Dimens. Syst. Nanostruct. 41 (2009) 1522–1526, https://doi.org/10.1016/j.physe.2009.04.027.

[13] Z. Zeng, C.S. Garoufalis, S. Baskoutas, Combination effects of tilted electric and magnetic fields on donor binding energy in a GaAs/AlGaAs cylindrical quantum dot, J. Phys. D, Appl. Phys. 45 (2012) 235102, https://doi.org/10.1088/0022-3727/45/23/235102.

[14] M. Barati, G. Rezaei, M.R.K. Vahdani, Binding energy of a hydrogenic donor impurity in an ellipsoidal finite-potential quantum dot, Phys. Status Solidi B 244 (2007) 2605–2610, https://doi.org/10.1002/pssb.200642543.

[15] H. Ham, C.J. Lee, H.N. Spector, Photoionization cross section of hydrogenic impurities in cylindrical quantum wires: infinite well model, J. Appl. Phys. 96 (2004) 335–339, https://doi.org/10.1063/1.1759394.

[16] E. Assaid, E. Feddi, M. Khaidar, F. Dujardin, B. Stébé, Electric field effect on the energy of an off-centre donor in quantum crystallites, Phys. Scr. 63 (2001) 329–335, https://doi.org/10.1238/Physica.Regular.063a00329.

[17] F. Dujardin, A. Oukerroum, E. Feddi, J. Bosch Bailach, J. Martinez-Pastor, M. Zazi, Effect of a lateral electric field on an off-center single dopant confined in a thin quantum disk, J. Appl. Phys. 111 (2012) 034317, https://doi.org/10.1063/1.3679144.

[18] A.L. Morales, A. Montes, S.Y. López, N. Raigoza, C.A. Duque, Donor-related density of states and polarizability in GaAs-(Ga, Al)As quantum-well under hydrostatic pressure and applied electric field, Phys. Status Solidi C 2 (2003) 652–656, https://doi.org/10.1002/pssc.200306176.

[19] A. Montes, C.A. Duque, Electric field effects on the states of a donor impurity in rectangular cross-section vacuum/GaAs/vacuum quantum-well wires 84 (1998) 1421, https://doi.org/10.1063/1.368176.

[20] H. Odiambo Oyoko, N. Porras-Montenegro, S.Y. Lopez, C.A. Duque, Comparative study of the hydrostatic pressure and temperature effects on the impurity-related optical properties in single and double GaAs-$Ga_{1-x}Al_xAs$ quantum wells, Phys. Status Solidi C 4 (2) (2007) 298–300, https://doi.org/10.1002/pssc.200673259.

[21] S. Baskoutas, E. Paspalakis, A.F. Terzis, Electronic structure and nonlinear optical rectification in a quantum dot: effects of impurities and external electric field, J. Phys. Condens. Matter 19 (2007) 395024, https://doi.org/10.1088/0953-8984/19/39/395024.

[22] M. Cristea, E.C. Niculescu, Hydrogenic impurity states in CdSe/ZnS and ZnS/CdSe core-shell nanodots with a dielectric mismatch, Eur. Phys. J. B 85 (2012) 191, https://doi.org/10.1140/epjb/e2012-21051-2.

[23] A. Chafai, I. Essaoudi, A. Ainane, F. Dujardin, R. Ahuja, Hydrogenic donor in a CdSe/CdS quantum dot: effect of electric field strength, nanodot shape and dielectric environment on the energy spectrum, Physica E, Low-Dimens. Syst. Nanostruct. 104 (2018) 29–35, https://doi.org/10.1016/j.physe.2018.07.010.

[24] H. Ham, H.N. Spector, Photoionization cross section of hydrogenic impurities in cylindrical quantum wires: finite well model, J. Appl. Phys. 100 (2006) 024304, https://doi.org/10.1063/1.2211311.

[25] S. M'zerd, M. El Haouari, M. Aghoutane, M. El-Yadri, E. Feddi, F. Dujardin, I. Zorkani, A. Jorio, M. Sadoqi, G. Long, Electric field effect on the photoionization cross-section of a single dopant in a strained AlAs/GaAs spherical core/shell quantum dot, J. Appl. Phys. 124 (2018) 164303, https://doi.org/10.1063/1.5046859.

[26] V. Holovatsky, M. Chubrey, O. Voitsekhivska, Effect of electric field on photoionization cross-section of impurity in a multilayered quantum dot, Superlattices Microstruct. 145 (2020) 106642, https://doi.org/10.1016/j.spmi.2020.106642.

[27] A. Ed-Dahmouny, N. Zeiri, A. Fakkahi, R. Arraoui, M. Jaouane, A. Sali, N. Es-Sbai, K. El-Bakkari, C.A. Duque, Impurity photo-ionization cross-section and Stark shift of ground and two low-lying excited electron-states in a core/shell ellipsoidal quantum dot, Chem. Phys. Lett. 812 (2023) 140251, https://doi.org/10.1016/j.cplett.2022.140251.

[28] M. Şahin, F. Tek, A. Erdinç, The photoionization cross-section of a hydrogenic impurity in a multi-layered spherical quantum dot, J. Appl. Phys. 111 (2012) 084317, https://doi.org/10.1063/1.4705410.

[29] L. Shi, Z.W. Yan, Stark shift and photoionization cross section of on-center and off-center donor impurity in a core/shell ellipsoidal quantum dot, Physica E, Low-Dimens. Syst. Nanostruct. 98 (2018) 111–117, https://doi.org/10.1016/j.physe.2017.12.034.

[30] A. Fakkahi, M. Jaouane, K. Limame, A. Sali, M. Kirak, R. Arraoui, A. Ed-Dahmouny, K. El-bakkari, H. Azmi, The impact of the electric field on the photoionization cross-section, polarizability, and donor impurity binding energy in multilayered spherical quantum dots, Appl. Phys. A 129 (2023) 188, https://doi.org/10.1007/s00339-023-06472-w.

[31] C. Delerue, M. Lannoo, Nanostructures: Theory and Modelling, Springer-Verlag Berlin Heidelberg, 2004.

[32] Z. Zeng, C.S. Garoufalis, A.F. Terzis, S. Baskoutas, Linear and nonlinear optical properties of ZnO/ZnS and ZnS/ZnO core-shell quantum dots: effects of shell thickness, impurity, and dielectric environment, J. Appl. Phys. 114 (2013) 023510, https://doi.org/10.1063/1.4813094.

[33] N. Zeiri, A. Naifar, S. Abdi-Ben Nasrallah, M. Said, Third nonlinear optical susceptibility of CdS/ZnS core-shell spherical quantum dots for optoelectronic devices, Optik 176 (2019) 162–167, https://doi.org/10.1016/j.ijleo.2018.09.050.

[34] L. Shi, Z.W. Yan, Electric field and shape effect on the linear and nonlinear optical properties of multi-shell ellipsoidal quantum dots, Superlattices Microstruct. 94 (2016) 204–214, https://doi.org/10.1016/j.spmi.2016.04.022.

[35] M. El Haouari, A. Talbi, E. Feddi, H. El Ghazi, A. Oukerroum, F. Dujardin, Linear and nonlinear optical properties of a single dopant in strained AlAs/GaAs spherical core/shell quantum dots, Opt. Commun. 383 (2017) 231–237, https://doi.org/10.1016/j.optcom.2016.09.019.

[36] A. Chafai, I. Essaoudi, A. Ainane, R. Ahuja, Linear and nonlinear optical properties of donors inside a CdSe/ZnTe core/shell nanodot: role of size modulation, Results Phys. 14 (2019) 102414, https://doi.org/10.1016/j.rinp.2019.102414.

[37] F.K. Boz, B. Nisanci, S. Aktas, S.E. Okan, Energy levels of GaAs/$Al_xGa_{1-x}As$/AlAs spherical quantum dot with an impurity, Appl. Surf. Sci. 387 (2016) 76–81, https://doi.org/10.1016/j.apsusc.2016.06.035.

[38] A. Oukerroum, M. El-Yadri, A. El Aouami, E. Feddi, F. Dujardin, C.A. Duque, M. Sadoqi, G. Long, Oscillator strength and quantum-confined Stark effect of excitons in a thin PbS quantum disk, Int. J. Mod. Phys. B 32 (2018) 1750266, https://doi.org/10.1142/S0217979217502666.

[39] L.M. Burileanu, Photoionization cross-section of a donor impurity in spherical quantum dots under electric and intense laser fields, J. Lumin. 145 (2014) 684–689, https://doi.org/10.1016/j.jlumin.2013.08.043.

[40] D.B. Hayrapetyan, G.L. Ohanyan, D.A. Baghdasaryan, H.A. Sarkisyan, S. Baskoutas, E.M. Kazaryan, Binding energy and photoionization cross-section of a hydrogen-like donor impurity in a strongly oblate ellipsoidal quantum dot, Physica E, Low-Dimens. Syst. Nanostruct. 95 (2018) 27–31, https://doi.org/10.1016/j.physe.2017.09.006.

[41] A. Ed-Dahmouny, A. Sali, N. Es-Sbai, R. Arraoui, M. Jaouane, A. Fakkahi, K. El-Bakkari, C.A. Duque, Combined effects of hydrostatic pressure and electric field on the donor binding energy, polarizability, and photoionization cross-section in double GaAs/$Ga_{1-x}Al_xAs$ quantum dots, Eur. Phys. J. B 95 (2022) 136, https://doi.org/10.1140/epjb/s10051-022-00400-2.

[42] S. Li, L. Shi, Z.W. Yan, Binding energies and photoionization cross-sections of donor impurities in GaN/$Al_xGa_{1-x}N$ spherical quantum dot under hydrostatic pressure, Mod. Phys. Lett. B 34 (2020) 2050153, https://doi.org/10.1142/S0217984920501535.

[43] S. Hértilli, N. Yahyaoui, N. Zeiri, S. Saadaoui, M. Said, Energy levels and nonlinear optical properties of spheroid-shaped CdTe/ZnTe core/shell quantum dot,

Opt. Laser Technol. 155 (2022) 108425, https://doi.org/10.1016/j.optlastec.2022.108425.
[44] B. Kumar, B.K. Kaushik, Y.S. Negi, Perspectives and challenges for organic thin film transistors: materials, devices, processes and applications, J. Mater. Sci., Mater. Electron. 25 (2014) 1–30, https://doi.org/10.1007/s10854-013-1550-2.
[45] A. Cherni, N. Yahyaoui, N. Zeiri, M. Said, S. Saadaoui, Simultaneous effect of the capped matrix and the geometric factors of CdS/ZnSe spheroidal quantum dots on the linear and nonlinear optical properties, Opt. Quantum Electron. 55 (2023) 273, https://doi.org/10.1007/s11082-023-04545-x.
[46] M. Hbibi, O. Mommadi, S. Chouef, R. Boussetta, L. Belamkadem, A. El Moussaouy, F. Falyouni, C.M. Duque, J.A. Vinasco, Finite confinement potentials, core and shell size effects on excitonic and electron-atom properties in cylindrical core/shell/shell quantum dots, Sci. Rep. 12 (2022) 14854, https://doi.org/10.1038/s41598-022-19118-3.
[47] A. Sivakami, V. Gayathri, Hydrostatic pressure and temperature dependence of dielectric mismatch effect on the impurity binding energy in a spherical quantum dot, Superlattices Microstruct. 58 (2013) 218–227, https://doi.org/10.1016/j.spmi.2013.03.002.
[48] A. Chafai, F. Dujardin, I. Essaoudi, A. Ainane, R. Ahuja, Shallow donor inside core/shell spherical nanodot: effect of nanostructure size and dielectric environment on the energy spectrum, Superlattices Microstruct. 111 (2017) 976–982, https://doi.org/10.1016/j.spmi.2017.07.063.
[49] M. Elamathi, A. John Peter, C.W. Lee, Role of various dielectric environment matrices of InP/ZnS core/shell quantum dot on optical gain coefficient, Eur. Phys. J. D 74 (2020) 196, https://doi.org/10.1140/epjd/e2020-10095-6.
[50] E.C. Niculescu, M. Cristea, Impurity states and photoionization cross section in CdSe/ZnS core-shell nanodots with dielectric confinement, J. Lumin. 135 (2013) 120–127, https://doi.org/10.1016/j.jlumin.2012.10.032.
[51] Z. Zeng, C.S. Garoufalis, S. Baskoutas, A.F. Terzis, Stark effect of donor binding energy in a self-assembled GaAs quantum dot subjected to a tilted electric field, Phys. Lett. A 376 (2012) 2712–2716, https://doi.org/10.1016/j.physleta.2012.07.032.
[52] L. Aderras, A. Bah, E. Feddi, F. Dujardin, C.A. Duque, Stark-shift of impurity fundamental state in a lens-shaped quantum dot, Physica E, Low-Dimens. Syst. Nanostruct. 89 (2017) 119–123, https://doi.org/10.1016/j.physe.2017.02.012.
[53] A. Oukerroum, E. Feddi, J. Bosch Bailach, J. Martinez-Pastor, F. Dujardin, E. Assaid, On the anomalous Stark effect in a thin disc-shaped quantum dot, J. Phys. Condens. Matter 22 (2010) 375301, https://doi.org/10.1088/0953-8984/22/37/375301.
[54] N. Zeiri, A. Cherni, N. Yahyaoui, P. Baser, M. Said, S. Saadaoui, Photoionization cross-section and polarizability of impurity in CdS/ZnS core/shell quantum dots capped in a dielectric matrix, Solid State Commun. (2023) 115181, https://doi.org/10.1016/j.ssc.2023.115181.
[55] M. Cristea, E.C. Niculescu, Polarizability of a donor impurity in dielectrically modulated core-shell nanodots, Phys. Lett. A 377 (2013) 1221–1226, https://doi.org/10.1016/j.physleta.2013.03.012.
[56] E.C. Niculescu, Dielectric mismatch effect on the photoionization cross section and intersublevel transitions in GaAs nanodots, Opt. Commun. 284 (2011) 3298–3303, https://doi.org/10.1016/j.optcom.2011.02.071.
[57] Z. Zeng, C.S. Garoufalis, S. Baskoutas, Nonlinear optical absorption in colloidal CdS quantum dots: the role of dielectric environment, J. Nanoelectron. Optoelectron. 11 (2016) 615–619, https://doi.org/10.1166/jno.2016.1940.